Evaluating dual porosity of pelletized diatomaceous earth using bimodal soil-water characteristic curve functions

Craig A. Burger and Charles D. Shackelford

Abstract: Soil-water characteristic curve data for specimens containing either ~1 mm or ~2 mm diameter pellets of processed diatomaceous earth are measured using a variety of methods (Tempe cell, pressure plate, filter paper, and chilled-mirror psychrometer). The measured soil-water characteristic curve data are bimodal, reflecting both the microscopic porosity region within the individual pellets, or intrapellet porosity, and the macroscopic porosity region between the pellets, or interpellet porosity. The bimodal distributions are consistent with scanning electron micrographs that show the existence of microscopic pores within each pellet, and the relatively high total porosities (0.725 and 0.764) for the coarse-grained diatomaceous earth specimens. The measured soil-water characteristic curve data are fit with modified forms of the Brooks–Corey, van Genuchten, and Fredlund–Xing soil-water characteristic curve functions to account for the bimodal shapes of the measured data. The average microscopic porosities resulting from the curve fits represent 45.0 and 47.9% of the total porosities for the two diatomaceous earth materials. These percentages of microscopic pore space are consistent with the product literature value of approximately 50% for the same materials based on mercury intrusion porosimetry. Thus, the results illustrate the application of bimodal soil-water characteristic curve functions for determining the microscopic and macroscopic portions of the total porosity of dual-porosity media, such as pelletized diatomaceous earth.

Key words: bimodal soil-water characteristic curves, diatomaceous earth, dual porosity, macroporosity, microporosity, soil-water characteristic curves (SWCC), soil suction.

Résumé : Les données de la courbe caractéristique sol-eau pour des spécimens contenant des granules de 1 mm à 2 mm de diamètre de terre diatomée sont mesurées au moyen d'une variété de méthodes (cellule Tempe, plaque de pression, papier filtre, et psychromètre à miroir froid). Les données mesurées de la courbe caractéristique sol-eau sont bimodales reflétant la région de porosité microscopique à l'intérieur des granules individuels, ou porosité intragranulaire, de même que la région de porosité macroscopique entre les granules, ou porosité intergranulaire. Les distributions bimodales sont consistantes avec les photographies au microscope électronique à balayage qui montrent l'existence de pores microscopiques à l'intérieur de chaque granule, et les porosités totales relativement élevées (0,725 et 0,764) pour les spécimens de terre diatomée à gros grains. Les mesures des données de la courbe caractéristique sol-eau sont ajustées aux formes modifiées des fonctions de courbe caractéristique sol-eau de Brooks–Corey, van Genuchten, et Fredlund–Xing pour tenir compte des formes bimodales des données mesurées. Les porosités microscopiques moyennes résultant des lissage de courbes représentent 45,0 % à 47,9 % des porosités totales pour les deux matériaux de terre diatomée. Ces pourcentages d'espace microscopique sont consistants avec la valeur de 50 % donnée pour ce produit dans la littérature pour les mêmes matériaux basées sur le porosimètre à intrusion de mercure. Ainsi, les résultats illustrent l'application des fonctions de courbes caractéristiques bimodales sol-eau pour déterminer les portions microscopiques et macroscopiques de la porosité totale des milieux à double porosité, tels que la terre granulée diatomée.

Mots clés : courbes caractéristiques sol-eau bimodales, terre diatomée, porosité double, macroporosité, microporosité, courbes caractéristiques sol-eau (SWCC), succion dans le sol.

[Traduit par la Rédaction]

Introduction

Natural diatomaceous earth, also known as diatomite, is a sedimentary deposit formed from the inorganic skeletal remains of single-cell algae and plankton. Dead algae and plankton, called diatoms, settle on the bottom of seas and lakes and form layers of diatomaceous earth. The organic matter decays and the shells form a deposit with interconnected

Received January 4, 2000. Accepted August 1, 2000. Published on the NRC Research Press Web site on February 14, 2001.

C.A. Burger[1] and C.D. Shackelford. Department of Civil Engineering, Colorado State University, Fort Collins, CO 80523-1372, U.S.A.

[1]Present address: Montgomery Watson Mining Group, 165 South Union Boulevard, Suite 410, Lakewood, CO 80228, U.S.A.

 DOI: 10.1139/cgj-38-1-53

pores of sizes appropriate for microbiological growth and filtering of solids suspended in water. The structure and distribution of these interconnected pores result in a relatively high porosity (typically >70%) and high surface area (Breese 1994). This naturally occurring diatomaceous earth has been used as engineered fill in California (Khilnani and Capik 1989; Day 1995). The diatomaceous earth layers also are mined and processed to segregate the particles by size and remove impurities for commercial use.

In the process of mining diatomaceous earth for industrial applications, the diatomaceous earth deposits first are crushed into aggregate sizes before being subjected to a mill drying process that results in smaller particle sizes. The diatomaceous earth then is packed as a natural milled product for use as a filter aid and filler material to enhance and alter material properties (Meisinger 1985; Breese 1994). If the diatomaceous earth is to be used as a filter material, further processing, known as either calcination (thermal processing) or flux calcination (calcination with a fluxing agent), may be necessary to increase the permeability. In the process of calcination, the particles of diatomaceous earth are bonded together to form larger particle sizes (Lange 1983; Breese 1994). A range of particle sizes from powder to pellets several millimetres in diameter can be produced in the calcination process. Other properties of diatomaceous earth pertaining to industrial applications are described by Breese (1994) and Meisinger (1985).

The majority of mined and processed diatomaceous earth is used in filter applications to separate suspended solids from fluids (Breese 1994). These applications include filtering of solvents, pharmaceuticals, beer, wine, whiskey, raw sugar, liquors, antibiotics, and industrial, municipal, and swimming pool waters. Diatomaceous earth also is used as a biological growth medium for microorganisms in biological filtration, a soil amendment to increase drainage and water-holding capacity, and a hydroponic medium for plant growth. For example, Lukasik et al. (1996) evaluated the use of diatomaceous earth coated with metal hydroxides to improve adsorption of microorganisms during biological filtration. In addition, diatomaceous earth recently has been used for bioremediation of contaminated soil and as the biological growth medium in constructed wetlands for runoff treatment (Stavnes et al. 1996; Sundine Enterprises, Inc. 1996).

For aggregated diatomaceous earth, two distinct pore-size distributions commonly exist, one for the macroscopic porosity region between the particles (interpellet porosity) and another distribution for the microscopic porosity region within the particles (intrapellet porosity). The existence of two distinct pore-size distributions in other porous media has resulted in the measurement of bimodal soil-water characteristic curves. In the majority of studies, bimodal soil-water characteristic curves have been observed for structured soils, such as aggregated loams (Smettem and Kirby 1990; Wilson et al. 1992; Durner 1994; Mallants et al. 1997). Othmer et al. (1991) attributed the observation of bimodal soil-water characteristic curves for a fluvial loess deposit to the existence of wormholes resulting in "vertical tubular macropores." Bimodal soil-water characteristic curves also have been observed for porous media that exhibit significant secondary structure, such as fractured tuff (Peters and Klavetter 1988; Pruess et al. 1990; Wang and Narasimhan 1985, 1990).

Based on the bimodal pore-size distributions typically associated with naturally occurring, aggregated diatomaceous earth, the soil-water characteristic curves for commercially processed, pelletized diatomaceous earth also are expected to be bimodal. Thus, the hypothesis for this study is that the soil-water characteristic curves for pelletized diatomaceous earth are bimodal and, therefore, can be used to distinguish the secondary, intrapellet or microscopic porosity from the primary, interpellet or macroscopic porosity by fitting the data with appropriate soil-water characteristic curve functions. This hypothesis will be evaluated by measuring the soil-water characteristic curve data of two pelletized diatomaceous earth materials using several different methods of measurement to cover a broad range of suctions. The measured data will be analyzed using several soil-water characteristic curve functions to determine the percentages of the pore space that can be attributed to the microscopic porosity and the macroscopic porosity. The overall objective of this study is to determine the potential use of various bimodal soil-water characteristic curve functions for providing an independent assessment of the percentage of the total porosity that can be attributed to the microporosity and macroporosity regions of dual-porosity media. Such an assessment would provide an alternative to other methods, such as mercury-intrusion porosimetry, and also would be beneficial, for example, in terms of the use of dual-porosity models to simulate water and solute migration through dual-porosity media (e.g., Gerke and van Genuchten 1993; Maraqa et al. 1997; Ray et al. 1997; Griffioen et al. 1998).

Materials and methods

Materials

A processed diatomaceous earth was used in this study. The processed diatomaceous earth is a commercial product with the trade name Isolite® distributed by Sundine Enterprises, Inc. (Denver, Colo.) under the product names CG1 and CG2 corresponding to average pellet diameters of approximately 1 and 2 mm, respectively. The actual particle-size distributions (American Society for Testing and Materials (ASTM) D422) for the CG1 and CG2 pellets are shown in Fig. 1, and the coarse texture of the CG1 and CG2 pellets is illustrated in Fig. 2. The pellets are formed by extruding crushed diatomaceous earth through holes followed by a calcination process to bond the diatoms together. The material is kiln fired at 980°C (1800°F) in the calcination process.

Scanning electron micrographs showing the existence of microscopic pores in the CG1 and CG2 pellets are presented in Fig. 3. The pore-size distributions of the microscopic portions of the CG1 and CG2 pellets determined by mercury-intrusion porosimetry (ASTM D4404) based on the product literature are given in Table 1. This microscopic porosity typically accounts for approximately 50% of the total (bulk) porosity for CG1 and CG2 pellets, with the actual percentage depending on the relative density of the pellets (Sundine Enterprises, Inc. 1996).

The measured specific gravity (ASTM D854), maximum dry density (ASTM D4253), and minimum dry density (ASTM D4254) for the CG1 pellets were 2.28, 0.537 g/cm^3, and 0.506 g/cm^3, respectively. The measured specific gravity (ASTM D854), maximum dry density (ASTM D4253), and

Fig. 1. Particle-size distributions (ASTM D422) for two different pellet sizes of processed diatomaceous earth (CG1 and CG2).

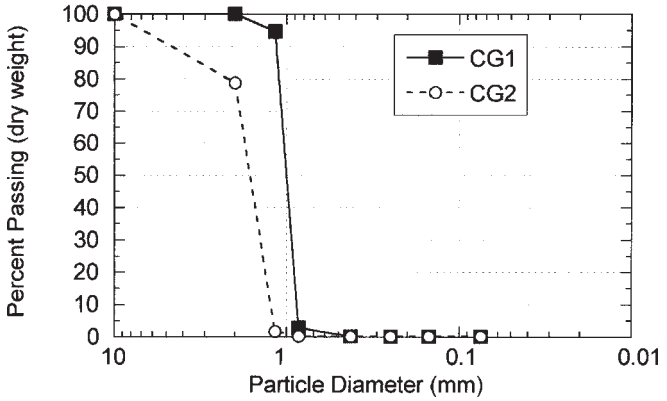

minimum dry density (ASTM D4254) for the CG2 pellets were 2.24, 0.617 g/cm^3, and 0.584 g/cm^3, respectively. Both CG1 and CG2 classify as poorly graded sands (SP) according to ASTM D2487, and simply as sands based on the U.S. Department of Agriculture classification.

The chemical composition of Isolite® by weight is 78% SiO_2, 12% Al_2O_3, and 5% Fe_2O_3, with all other chemicals making up less than 5%. A sulfate soundness test (ASTM C88) resulted in 2% loss, indicating that Isolite® is chemically and physically inert (Sundine Enterprises, Inc. 1996).

Experimental methods and analyses

Measurement of soil-water characteristic curves

Four methods were used to measure the soil-water characteristic curve data for the CG1 and CG2 materials reported in this study: (*i*) the Tempe cell method, (*ii*) the pressure plate method, (*iii*) the filter paper method, and (*iv*) the chilled-mirror psychrometer method. The use of these four methods was based primarily on two considerations: (*i*) the need to measure soil-water characteristic curve data over a wide range of suctions, and (*ii*) the desire to measure the soil-water characteristic curve data within a reasonable period (≤8 days).

Tempe cells (model 1400, Soil Moisture Co., Santa Barbara, Calif.) were used to measure soil-water characteristic curve data for matric suction values less than 3.4 kPa. Soil-water characteristic curve data for low suctions are required to provide a well-defined soil-water characteristic curve for coarse-grained materials such as pelletized diatomaceous earth. The measurements using the Tempe cells reached equilibrium within 24 h.

A pressure plate apparatus (model 1600, Soil Moisture Co.) was used to measure matric suction values between 3.4 and 100 kPa based on the procedures described in ASTM D2325. The use of the pressure plate apparatus was restricted to data corresponding to suctions ≤100 kPa because data for higher suctions would have required more than 8 days to equilibrate. Although Klute (1986) indicates that equilibrium conditions (no outflow of water from the soil) using a pressure plate occur in a 20–30 mm high soil specimen within 2–3 days for most soil types, others have found that equilibrium may take much longer (Chao 1995; Rogers and Gallaher 1995; Miller 1996). For example, the time required to achieve equilibrium for measurements using clays ranged from 20 to 25 days for Chao (1995) and from 7 to 14 days for Miller (1996). These relatively long times probably reflect the low unsaturated hydraulic conductivity that typically results at high suctions in clays, or in any soil at a low degree of saturation.

Fig. 2. Photograph showing coarse texture of CG1 (left) and CG2 (right) pellets.

Table 1. Pore-size distribution (%) of the microscopic (intrapellet) porosity portion of CG1 and CG2 pelletized diatomaceous earth from mercury-intrusion porosimetry (Sundine Enterprises, Inc. 1996).

Range in pore sizes (μm)	CG1	CG2
<0.5	9	6
0.5–1.0	19	12
1.0–2.0	33	27
2.0–3.0	12	16
3.0–4.0	5	7
4.0–5.0	4	4
>5.0	18 (to 20.47 μm)	28 (to 16.67 μm)
Total	100	100

The times required to reach equilibrium using the pressure plate apparatus in this study for CG1 and matric suctions of 100 kPa (1 bar) and 230 kPa (2.3 bar) are shown in Fig. 4. The data in Fig. 4 indicate that equilibrium is achieved at approximately 8 days for the lower suction of 100 kPa, but is not attained within 14 days for the higher suction of 230 kPa. Water in the macroporosity region between individual pellets probably drains rapidly, whereas the water in the microporosity region within each pellet probably is held more tightly due to the smaller pores and more tortuous paths for water flow. In addition, the water phase may become discontinuous around an individual diatomaceous earth pellet, preventing outflow of water from within the pellet. This effect results in erroneously high water contents for the applied matric suction.

As previously noted, all pressure plate data were obtained on separate, individually prepared specimens of the diatomaceous earth. As shown in Fig. 5, preliminary pressure plate measurements performed on duplicate specimens of both CG1 and CG2 indicated that reproducibility of the

Fig. 3. Scanning electron micrographs showing microscopic pores in CG1 and CG2 diatomaceous earth pellets: (*a*) CG1; (*b*, *c*) CG2. Each interval on the scales represents 10 μm.

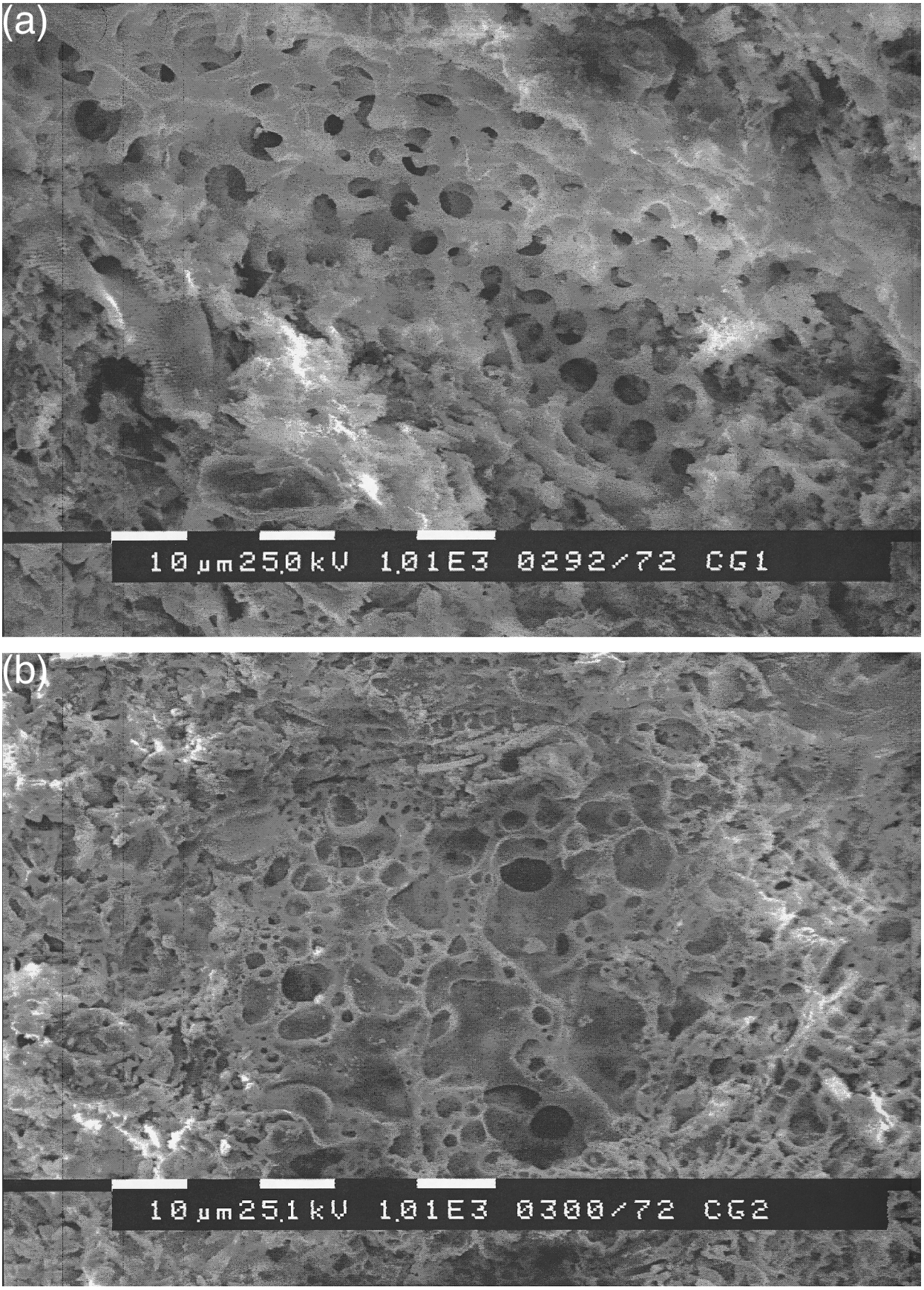

Fig. 3 (*concluded*).

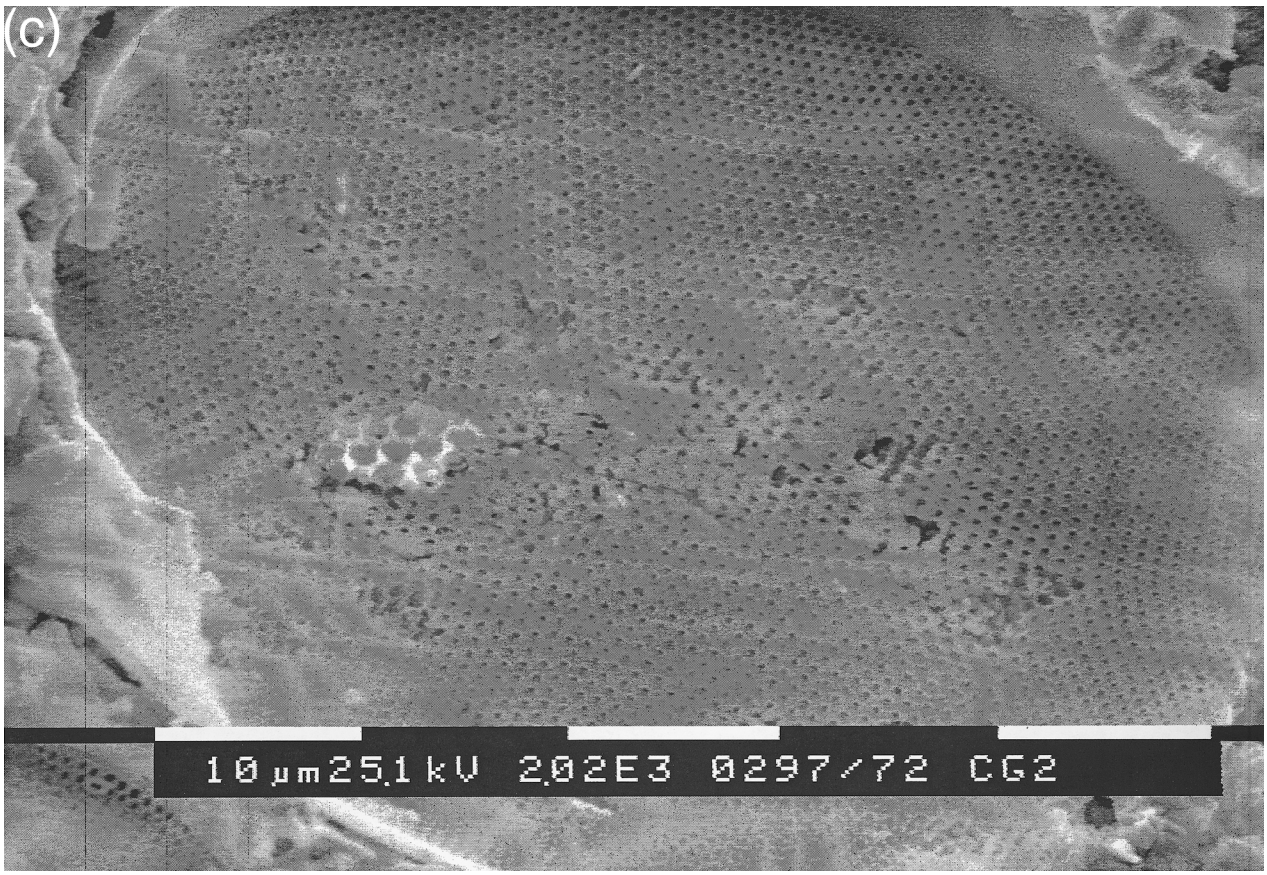

Fig. 4. Time to achieve equilibrium for pressure plate tests on CG1 diatomaceous earth pellets.

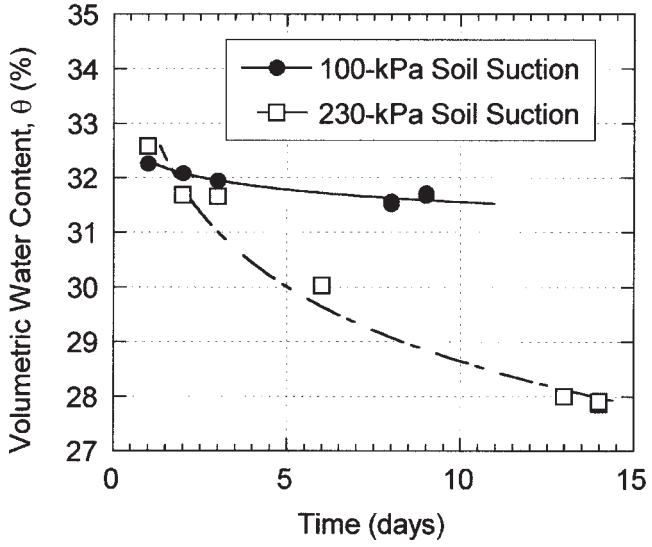

measured volumetric water contents at a given suction generally was very good.

As a result of the long times required to reach equilibrium at relatively high suctions in the pressure plate method for CG1, soil-water characteristic curve data for total suction values greater than 196 kPa of water were obtained using the filter paper method. No soil-water characteristic curve data were measured for suctions between 100 and 196 kPa. The filter paper method (ASTM D5298) measures the total (matric plus osmotic) suction of a dry soil within 7 days.

A calibration curve for the filter paper test was developed by measuring the gravimetric water content of filter papers in equilibrium with salt solutions with a known osmotic suction value that can be calculated from the molality of the solution. The measured calibration curve for Whatman No. 42, quantitative, ashless, 42.5 mm circular filter papers used in this study is shown in Fig. 6. No calibration data were measured for suctions less than 20 m of water (196 kPa). The measured calibration curve is offset significantly from the calibration curve suggested by ASTM D5298. This difference could be caused by the use of a different diameter of Whatman No. 42 filter paper, or by a difference in the amount of water that evaporated from the filter paper during the time required to transfer the filter paper to a sealed water-content container. At suctions less than 50 m of water (490 kPa), the scatter in the measured calibration data appears to be greater. This trend of increasing scatter in the data with decreasing suction also has been observed in other measured calibrations using the filter paper method (Miller 1996).

Soil-water characteristic curve data for total suctions greater than ~400 kPa also were obtained using a chilled-mirror psychrometer (trade name Aqualab®, Decagon Devices, Pullman, Wash.) to check the filter paper results. The chilled-mirror psychrometer (CMP) measures the suction of a specimen in 3–5 min. The CMP measures the relative humidity above a specimen with a stainless steel mirror that is cooled until condensation occurs. The dew point temperature is detected by a change in the optical properties of the

mirror, and the relative humidity in equilibrium with the soil pore water is calculated based on the dew point temperature. The total suction then is calculated from the thermodynamic relationship between total suction and relative humidity. The CMP was designed for agricultural purposes and uses a small specimen size (7 cm^3). Additional details regarding the use of the CMP are provided by Gee et al. (1992), who concluded that the CMP is a rapid method for measuring suction values greater than ~400 kPa.

Specimen preparation

Suction measurements were performed at the maximum dry density (ASTM D4253) to reduce the effect of changes in dry density on the size of the macroscopic pores. First, the dimensions of the specimen containers were measured using a micrometer. These dimensions then were used to calculate the volumes of the specimen containers, and the amount of dry material corresponding to the product of the maximum dry density and volume of the specimen containers was determined. For measurements made using either the Tempe cell or the pressure plate, the mass of dry material corresponding to the maximum dry density was weighed to ±0.01 g, placed into the specimen rings in contact with the porous plate, compacted with static compaction, and saturated through the porous plate in accordance with ASTM D2325. For measurements made using either the filter paper method or the CMP, the amount of dry material corresponding to the maximum dry density was weighed to ±0.01 g. The resulting material was washed with deionized water (DIW) to remove soluble salts, saturated by immersion in DIW for 24 h, and air-dried until the desired water content was achieved. After completion of air drying, the material was placed into the specimen containers at the maximum dry density using static compaction. One lift was used for compaction of all specimens due to the relatively small dimensions of the specimen containers. For example, the maximum thickness of all the specimens corresponded to 10.2 cm for the filter paper specimens. Independent specimens were prepared for the measurement of each data point.

The total (bulk) porosity, n_T, of the resulting specimens was estimated on the basis of the measured maximum dry density (ρ_{dmax}) and specific gravity of solids (G_s) using the following equation:

$$[1] \qquad n_T = 1 - \frac{\rho_{dmax}}{G_s \rho_w}$$

where ρ_w is the density of water (~1 g/cm^3). The resulting total porosities for CG1 and CG2 were 0.764 and 0.725, respectively.

Soil-water characteristic curve functions

The soil-water characteristic curve is a function of the pore-size distribution of the material and exhibits hysteresis between wetting and drying cycles (Fredlund and Rahardjo 1993). The soil-water characteristic curve commonly is plotted as the logarithm of soil suction (ψ) versus volumetric water content (θ). When dissolved salt concentrations are low such that the osmotic suction component of the soil suction is negligible, the soil suction essentially is the same as the matric suction (Fredlund and Rahardjo 1993).

Fig. 5. Reproducibility of measured volumetric water contents for duplicate specimens of CG1 and CG2 diatomaceous earth pellets at various applied matric suctions.

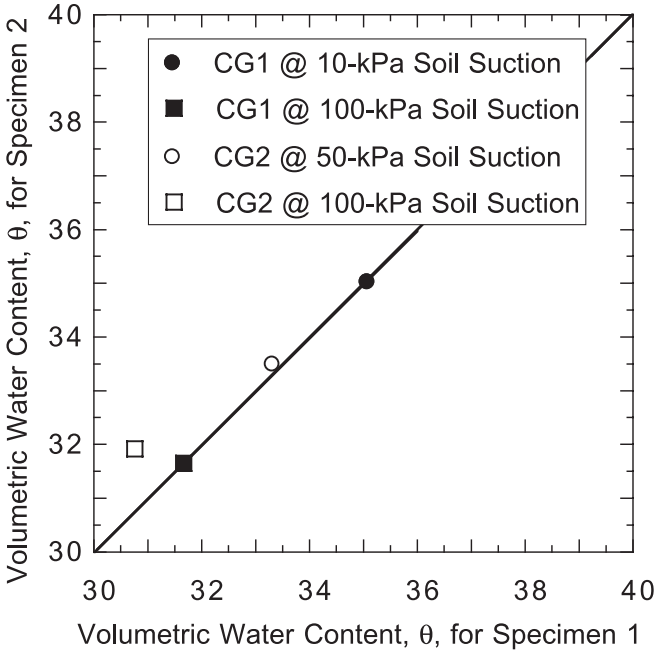

Soil-water characteristic curve functions commonly are used to describe the trends in soil-water characteristic curve data. The soil-water characteristic curve functions presented by Brooks and Corey (1964), van Genuchten (1980), and Fredlund and Xing (1994) were considered for use in this study. The Brooks–Corey function and the van Genuchten function were considered because these two functions commonly are used in simulating unsaturated flow through porous media. The Fredlund–Xing function also was considered for use because it reportedly provides a better description of the soil-water characteristic curve over a wide range of suctions (Leong and Rahardjo 1997).

The Brooks–Corey function may be written as follows (Brooks and Corey 1964):

$$[2] \qquad \theta = \begin{cases} \theta_r + (\theta_s - \theta_r)\left(\dfrac{\psi}{\psi_d}\right)^{-\lambda} & ; \quad \psi_d < \psi \\ \theta_s & ; \quad \psi \le \psi_d \end{cases}$$

where θ is the volumetric water content, θ_r is the residual water content, θ_s is the saturated water content, ψ_d is the air-entry or displacement suction, and λ is a fitting parameter known as the pore-size distribution index. The residual volumetric water content (θ_r) is defined by Fredlund and Rahardjo (1993) as the volumetric water content at which a change in suction produces an insignificant change in water content. The saturated volumetric water content (θ_s) is the maximum volumetric water content. The air-entry suction is higher for soils with smaller pore sizes. The pore-size distribution index decreases as the range of pore sizes increases, resulting in a steeper slope of the soil-water characteristic curve at suctions greater than the air-entry suction (e.g., Chiu and Shackelford 1998).

The van Genuchten function may be written as follows (van Genuchten 1980):

Fig. 6. Comparison of measured and ASTM D5298 filter paper calibrations for soil suction.

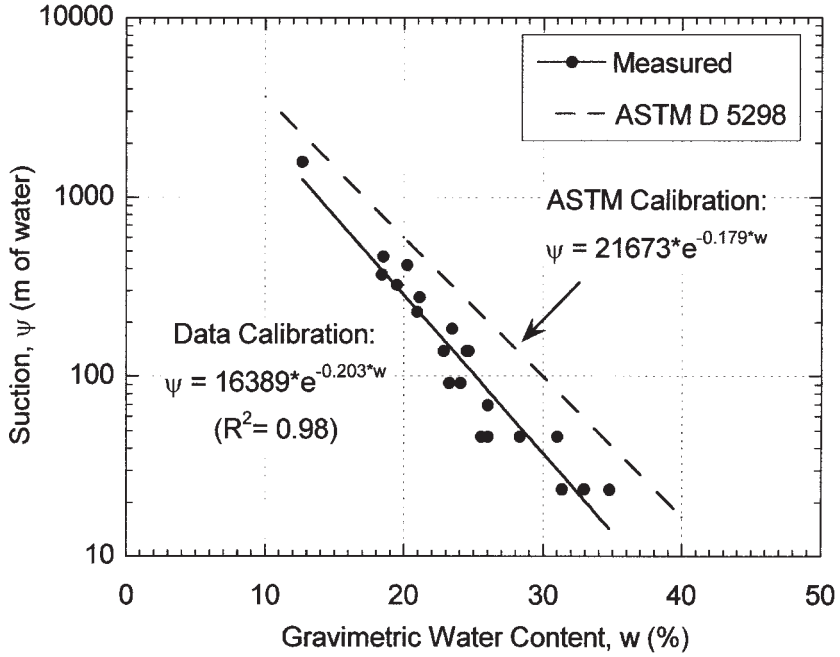

$$[3] \qquad \theta = \theta_r + (\theta_s - \theta_r)\left[\frac{1}{1+(\alpha\psi)^{\beta}}\right]^{m}$$

where α, β, and *m* are fitting parameters. Van Genuchten (1980) used the constraint that *m* is equal to 1 – 1/β to reduce the equation to two fitting parameters (α and β).

Each of the fitting parameters affects the soil-water characteristic curve differently. Although 1/α commonly is mistakenly assumed to represent the air-entry suction (e.g., Leong and Rahardjo 1997), van Genuchten (1980) notes that 1/α approaches the air-entry suction as *m* approaches unity (or as β approaches infinity) and, therefore, is related to the air-entry suction. A decrease in α shifts the soil-water characteristic curve to higher suctions for a given θ, whereas the slope of the soil-water characteristic curve at the inflection point decreases as β increases. The curvature of the soil-water characteristic curve at water contents near residual suction increases as *m* increases.

The Fredlund-Xing function may be written as follows (Fredlund and Xing 1994):

$$[4] \qquad \theta = C(\psi)\frac{\theta_s}{\left\{\ln\left[e+\left(\frac{\psi}{a}\right)^{n}\right]\right\}^{m}}$$

where $C(\psi)$ is a correcting function; e is the base of the natural logarithm; ψ is the soil suction (kPa); *a* represents the suction (kPa) at the inflection point in the soil-water characteristic curve and therefore is the same as the van Genuchten parameter 1/α; *n* is a parameter that controls the slope at the inflection point in the soil-water characteristic curve; and *m* is a parameter related to θ_r. Fredlund and Xing (1994) state that for smaller values of *m*, the parameter *a* is closer to the air-entry suction, which is consistent with the relationship between *m* and 1/*a* in the van Genuchten function. The correcting function, $C(\psi)$, has the following form:

$$[5] \qquad C(\psi) = 1 - \frac{\ln\left(1+\frac{\psi}{\psi_r}\right)}{\ln\left(1+\frac{10^6}{\psi_r}\right)}$$

where ψ_r is the residual suction (kPa), which is defined as the suction corresponding to the residual water content.

Soil-water characteristic curves that might be expected for sand, silt, and clay soils as described by the Brooks–Corey, van Genuchten, and Fredlund–Xing functions are shown in Fig. 7. The values for these curves were selected from the default fitting parameters in the RETC (Retention Curve) code (van Genuchten et al. 1991). The Brooks–Corey function is discontinuous at the air-entry suction, whereas the van Genuchten and Fredlund–Xing functions are continuous functions that smooth the predicted curve near the air-entry suction. The Fredlund–Xing function requires that a residual water content of zero occur at a suction of 10^6 kPa (Fredlund and Xing 1994).

Results

Soil-water characteristic curve data

All of the measured soil-water characteristic curve data for CG1 and CG2 is shown in Fig. 8. The filter paper and CMP data appear to compare reasonably well for suction values greater than ~400 kPa, and hysteresis between the drying and wetting cycles of the soil-water characteristic curves is not readily apparent based on the filter paper and CMP data.

The trend in the measured data in Fig. 8 also indicates that the soil-water characteristic curves for both the CG1 and CG2 materials are bimodal, as expected. The bimodal

Fig. 7. Unimodal soil-water characteristic curves for the Brooks–Corey, van Genuchten, and Fredlund–Xing functions for typical soils.

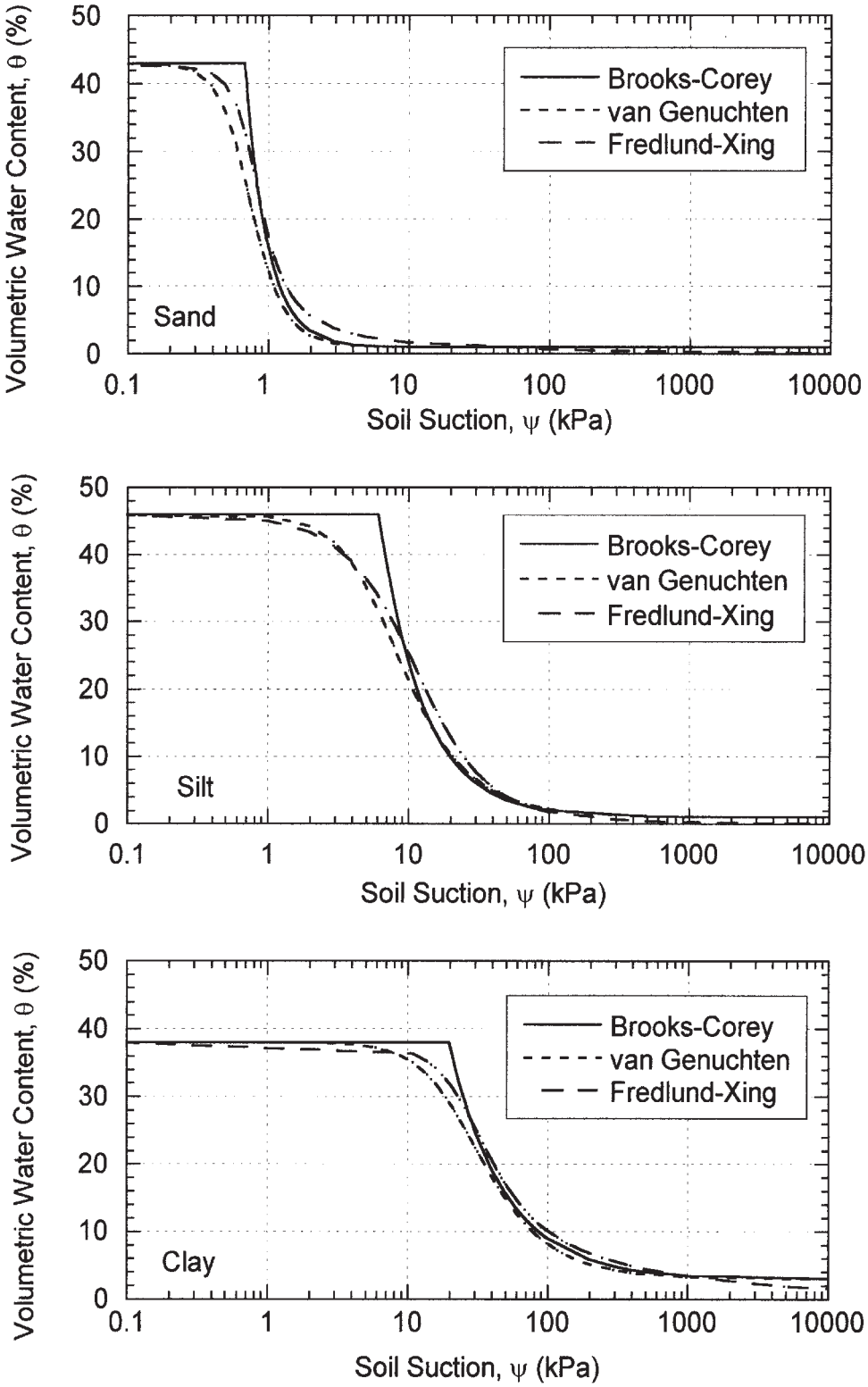

shapes of the soil-water characteristic curves are indicated both by the data corresponding to low suctions (≤1 kPa) measured using the Tempe cells and by the requirement that the soil-water characteristic curve approach the saturated volumetric water content (i.e., total porosity) for the materials at low suctions.

Soil-water characteristic curve fits

Since the Brooks–Corey, van Genuchten, and Fredlund–Xing functions defined by eqs. [2], [3], and [4], respectively, can be fit only to soil-water characteristic curve data for materials that exhibit a unimodal (bell-shaped) pore-size distribution, a modified fitting approach must be used to fit the

Fig. 8. Measured soil-water characteristic curve data for two different pellet sizes (CG1 and CG2) of processed diatomaceous earth based on several different methods of measurement.

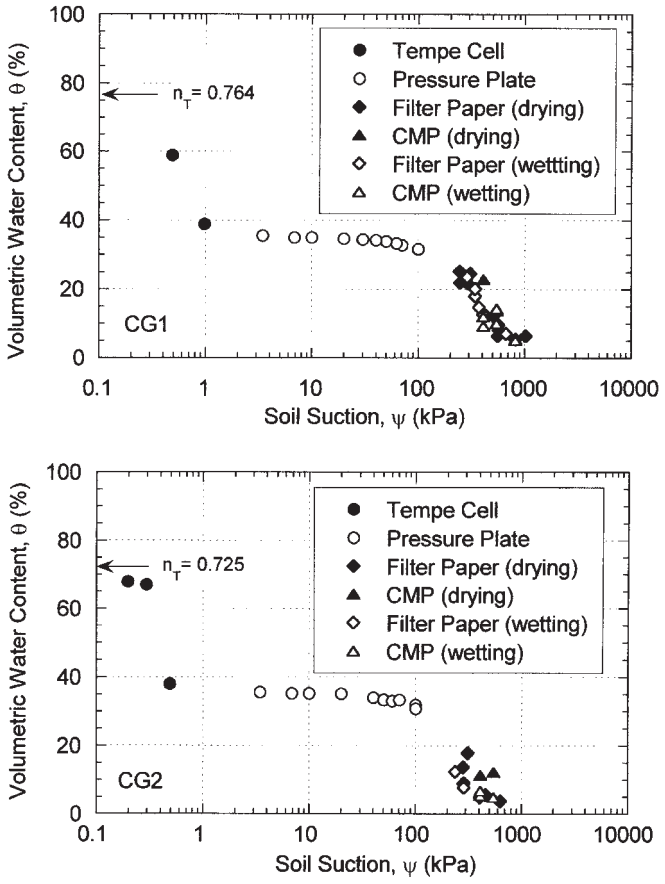

soil-water characteristic curve data measured in this study. In general, two approaches have been proposed to fit soil-water characteristic curve functions to bimodal soil-water characteristic curve data. The two proposed approaches heretofore have been based only on a modified form of the unimodal van Genuchten function.

The first approach is described by Smettem and Kirby (1990), Smettem et al. (1991), and Wilson et al. (1992). In this approach, the soil-water characteristic curve is separated into two regions joined at a common suction value, referred to as the matching point. The data in each region are fit separately using a unimodal soil-water characteristic curve function. The result is two sets of parameters with one set of parameters valid at suctions less than the common suction value and the other set of parameters valid at suctions greater than the common suction value.

The second approach, used by Othmer et al. (1991), Durner (1992, 1994), Ross and Smettem (1993), and Mallants et al. (1997), theoretically partitions the total porosity of the media into fractions accounting for the different pore-size distributions. Two unimodal functions, each associated with a fraction of the total porosity, are summed together to produce a single, total soil-water characteristic curve.

The method used in this study to fit the measured bimodal soil-water characteristic curve data observed for the CG1 and CG2 materials using the unimodal Brooks–Corey, van Genuchten, and Fredlund–Xing functions follows the procedure described by Smettem and Kirby (1990). This procedure can be explained further with the aid of the conceptual bimodal soil-water characteristic curve shown in Fig. 9. In this approach, a suction value, ψ_j, and corresponding volumetric water content, θ_j, were selected at the junction where the macroscopic porosity appears to have completely desaturated and the microscopic porosity begins to desaturate. Smettem and Kirby note that the selection of the exact position of this junction or matching point (ψ_j, θ_j) is somewhat arbitrary, but their experience with the approach has shown the procedure to be useful with respect to applications involving the determination of incipient ponding times and infiltration modeling. After selection of the junction point, the data for soil suctions greater than and less than ψ_j were fit separately, producing two sets of parameters. The RETC code was used to fit the Brooks–Corey and van Genuchten functions, and the SoilVision software package (SoilVision Systems Ltd., Saskatoon, Sask.) was used to fit the Fredlund–Xing function. For the RETC code, the θ_r value from the fit of data less than ψ_j is equal to θ_j. For the SoilVision software used to fit the Fredlund–Xing function, θ_r was not equal to θ_j, since the Fredlund–Xing function forces the water content to be zero at very high soil suctions.

Based on this approach, a bimodal soil-water characteristic curve can be described using the Brooks–Corey function as follows:

$$[6]\qquad \theta = \begin{cases} \theta_r + (\theta_j - \theta_r)\left(\dfrac{\psi}{\psi_d'}\right)^{-\lambda'} & ; \quad \psi_j < \psi \\ \theta_j + (\theta_s - \theta_j)\left(\dfrac{\psi}{\psi_d}\right)^{-\lambda} & ; \quad \psi_d < \psi \le \psi_j \\ \theta_s & ; \quad \psi \le \psi_d \end{cases}$$

where ψ_d and λ are the air-entry suction and the pore-size distribution index for the macroscopic portion of the data, respectively; and ψ_d' and λ' are the air-entry suction and the pore-size distribution fitting parameter for the microscopic portion of the data, respectively. When using the Brooks–Corey function for a bimodal soil-water characteristic curve, ψ_j is equal to ψ_d' due to the discontinuity in the function.

The bimodal soil-water characteristic curve can be described using the van Genuchten function with the constraint that $m = (1 - 1/\beta)$ as follows:

$$[7]\qquad \theta = \begin{cases} \theta_r + (\theta_j - \theta_r)\left[\dfrac{1}{1+(\alpha'\psi)^{\beta'}}\right]^{(1-1/\beta')} & ; \quad \psi_j < \psi \\ \theta_j + (\theta_s - \theta_j)\left[\dfrac{1}{1+(\alpha\psi)^{\beta}}\right]^{(1-1/\beta)} & ; \quad \psi \le \psi_j \end{cases}$$

where α and β are the fitting parameters for the macroscopic portion of the data, and α' and β' are the fitting parameters for the microscopic portion of the data.

The bimodal soil-water characteristic curve can be described using the Fredlund–Xing function in a manner similar to that of the van Genuchten function as follows:

$$[8]\qquad \theta = \begin{cases} C(\psi)\dfrac{\theta_j}{\left\{\ln\left[e+\left(\dfrac{\psi}{a'}\right)^{n'}\right]\right\}^{m'}} & ; \quad \psi_j < \psi \\ C(\psi)\dfrac{\theta_s}{\left\{\ln\left[e+\left(\dfrac{\psi}{a}\right)^{n}\right]\right\}^{m}} & ; \quad \psi \le \psi_j \end{cases}$$

where the correcting function has the following form:

$$[9]\qquad C(\psi) = \begin{cases} 1-\dfrac{\ln\left[1+\left(\dfrac{\psi}{\psi_r'}\right)\right]}{\ln\left[1+\left(\dfrac{10^6}{\psi_r'}\right)\right]} & ; \quad \psi_j < \psi \\ 1-\dfrac{\ln\left[1+\left(\dfrac{\psi}{\psi_r}\right)\right]}{\ln\left[1+\left(\dfrac{10^6}{\psi_r}\right)\right]} & ; \quad \psi \le \psi_j \end{cases}$$

and the prime symbol is used to indicate parameters that are fit to the microscopic portion of the data.

The bimodal Brooks–Corey and van Genuchten functions use two fitting parameters for each porosity region, whereas the bimodal Fredlund–Xing function uses four fitting parameters for each porosity region. Thus, the bimodal Fredlund–Xing function is expected to fit the measured soil-water characteristic curve data better than either the bimodal Brooks–Corey or van Genuchten functions.

Each of the bimodal soil-water characteristic curve functions was fit to all of the measured drying soil-water characteristic curve data for CG1 and CG2. For these curve fits, the saturated volumetric water content was assumed to equal the total porosity of the material (i.e., $\theta_s = n_T$). In addition, the osmotic suction component was assumed to be negligible due to the washing of soluble salts from the samples. As a result, the total suction values measured with the filter paper and CMP methods were assumed to be equal to the matric suction values. The resulting curve-fitted parameters based on each bimodal soil-water characteristic curve function are tabulated in Table 2 for both the microscopic (intrapellet) and macroscopic (interpellet) porosity regions of CG1 and CG2.

As shown by the values summarized in Table 2, the junction volumetric water content, θ_j, represents both the residual volumetric water content for the macroscopic portion of the data and the maximum volumetric water content for the microscopic portion of the data for the Brooks–Corey and the van Genuchten bimodal curve function fits. However, this constraint is not inherent in the Fredlund–Xing bimodal soil-water characteristic curve function. As a result, the residual volumetric water content resulting from fitting the Fredlund–Xing bimodal soil-water characteristic curve function to the macroscopic portion of the data, θ_r, actually is lower than maximum volumetric water content, or θ_j, for the microscopic portion of the data.

Table 2. Bimodal curve fit parameters for pelletized diatomaceous earth specimens CG1 and CG2.

Portion of soil-water characteristic curve	Parameter	CG1	CG2
Brooks–Corey function			
Microporosity	θ_r (%)	0.0	0.0
	θ_j (%)	34.4	34.4
	ψ_d' (kPa)	182	90.7
	λ'	0.93	0.85
	R^2	0.95	0.95
Macroporosity	θ_j (%)	34.4	34.4
	θ_s (%)	76.0	69.9
	ψ_d (kPa)	0.39	0.29
	λ	2.39	4.24
	R^2	0.99	0.99
Van Genuchten function			
Microporosity	θ_r (%)	0.0	0.0
	θ_j (%)	34.4	34.9
	α'	0.03	0.06
	β'	2.42	2.34
	R^2	0.95	0.95
Macroporosity	θ_j (%)	34.4	34.9
	θ_s (%)	76.0	70.0
	α	20.05	26.22
	β	4.12	9.24
	R^2	0.99	0.99
Fredlund–Xing function			
Microporosity	θ_r' (%)	0.1	4.9
	θ_j (%)	35.0	35.0
	a' (kPa)	568	124
	n'	1.71	4.36
	m'	3.96	0.74
	ψ_r' (kPa)	1082	370
	Error	0.09	0.09
Macroporosity	θ_r (%)	14.1	30.0
	θ_s (%)	76.0	72.0
	a (kPa)	0.47	0.30
	n	100	100
	m	0.15	0.15
	ψ_r (kPa)	15.9	1.8
	Error	<0.01	<0.01

Note: Error, sum of the squared residuals; R^2, coefficient of determination. All other fitting parameters as defined in the text.

The curve fits using the bimodal Brooks–Corey function (eq. [6]) for CG1 and CG2 are shown in Fig. 10. The bimodal Brooks–Corey function does not fit the curvature of the soil-water characteristic curve near the air-entry suction due to the discontinuity in the function. The curve fits using the bimodal van Genuchten function (eq. [7]) are shown in

Fig. 9. Schematic of a conceptual bimodal soil-water characteristic curve.

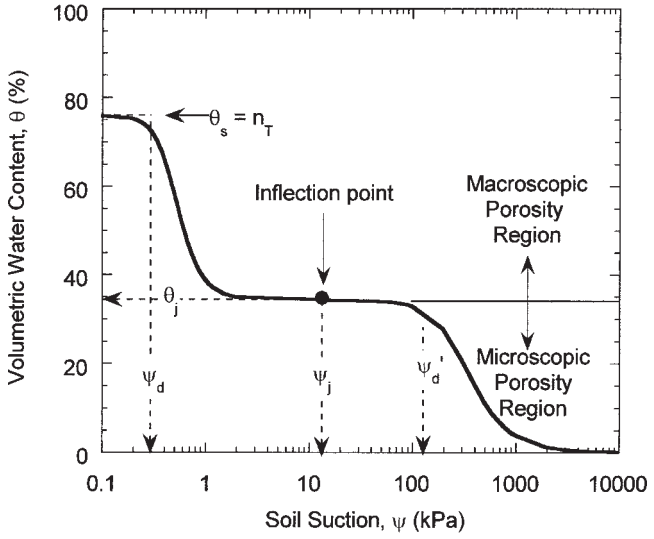

Fig. 11. The curvature near the air-entry suction is fit well, and the bimodal van Genuchten function visually appears to fit the data better than the bimodal Brooks–Corey function. The curve fits using the bimodal Fredlund–Xing function (eq. [8]) are shown in Fig. 12. The curvature near the air-entry suction also is fit well by the bimodal Fredlund–Xing function.

Comparison of air-entry suctions

The air-entry suctions (i.e., ψ_d and ψ_d') resulting from fitting the bimodal Brooks–Corey function to the measured soil-water characteristic curve data are compared in Fig. 13 with the values for $1/\alpha$ and $1/\alpha'$ resulting from the bimodal van Genuchten function fits and the values *a* and *a′* resulting from the bimodal Fredlund–Xing function fits to the same measured data. As previously noted, the van Genuchten parameters $1/\alpha$ and $1/\alpha'$ do not represent air-entry suctions, but the values of $1/\alpha$ and $1/\alpha'$ will approach the air-entry suctions as β and β', respectively, approach infinity. In a similar manner, the Fredlund–Xing parameters *a* and *a′* will approach the air-entry suction as *m* and *m′*, respectively, approach unity.

In general, the values for $1/\alpha$ and $1/\alpha'$ resulting from the bimodal van Genuchten function fits and the values for *a* and *a′* resulting from the bimodal Fredlund–Xing function fits are higher than the values for ψ_d and ψ_d' resulting from the bimodal Brooks–Corey function fits for both the microscopic and macroscopic portions of the soil-water characteristic curve. The values for ψ_d agree reasonably well with the values for $1/\alpha$ and *a*; however, there is a more significant difference between the values for ψ_d' and those for $1/\alpha'$ and *a′*. The better agreement between predictions for the macroscopic portion can be attributed, in part, to the similarity in shape of the curves generated by the different functions for the macroscopic portion of the soil-water characteristic curve.

Comparison of soil-water characteristic curves for CG1 and CG2

As shown in Fig. 8, the soil-water characteristic curves for the microscopic portions of CG1 and CG2 are similar. In

Fig. 10. Bimodal Brooks–Corey curve fits for specimens containing two different pellet sizes of processed diatomaceous earth (CG1 and CG2).

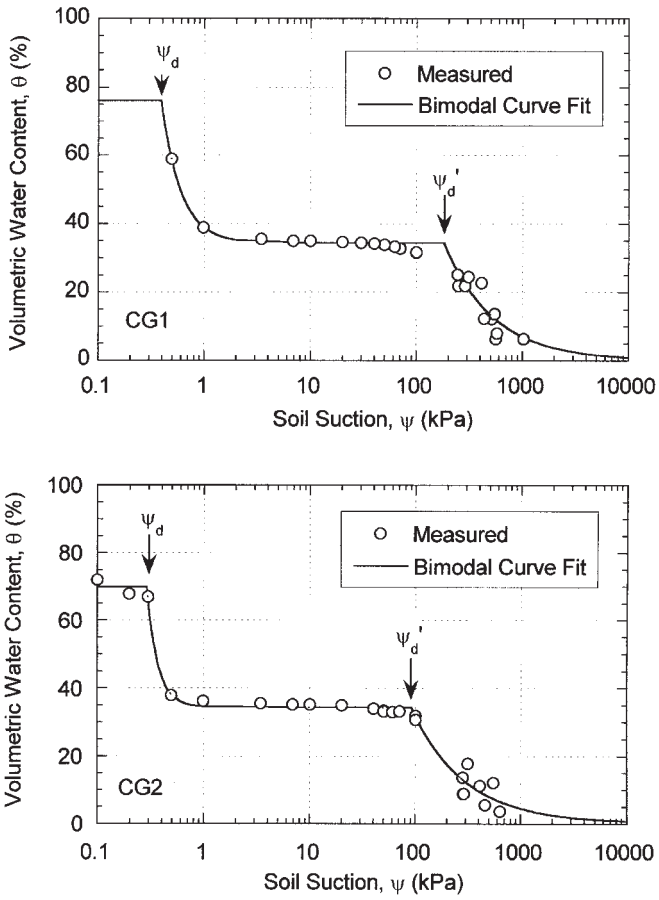

fact, there is no appreciable difference in the data sets for the microscopic portions of the data for these two materials. The microscopic portions of both materials begin to desaturate at approximately 100 kPa of suction. Overall, the microscopic pores for both materials desaturate between suctions of 100 and 980 kPa, implying that the microscopic portions of the materials contain a broad range of pore sizes. A broad range in pore sizes also is inferred by the low values for the microscopic pore-size distribution parameter, λ', from the Brooks–Corey function given in Table 2, i.e., since the pore-size distribution parameter theoretically approaches infinity when the pore size is uniform (Brooks and Corey 1964).

The soil-water characteristic curves for the macroscopic portions for CG1 and CG2 appear to be similar. However, the air-entry suction based on the macroscopic portion for CG2 is approximately 0.1 kPa lower than the air-entry suction based on the macroscopic portion for CG1 regardless of the fitting function used. This trend indicates slightly larger macroscopic pore sizes in the CG2 material than in the CG1 material, as expected on the basis of the slightly larger pellet sizes for CG2 (see Fig. 1).

Microscopic and macroscopic porosity

The portion of the total porosity of the material that can be attributed to the microscopic or intrapellet porosity, n_m, is assumed to be equal to the junction volumetric water

Fig. 11. Bimodal van Genuchten curve fits for specimens containing two different pellet sizes of processed diatomaceous earth (CG1 and CG2).

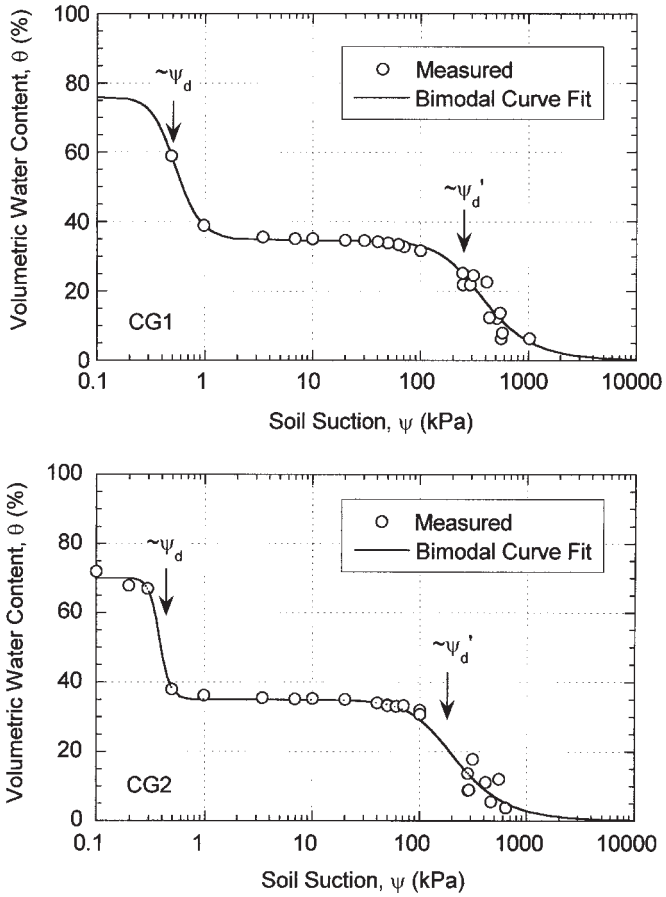

Fig. 12. Bimodal Fredlund–Xing curve fits for specimens containing two different pellet sizes of processed diatomaceous earth (CG1 and CG2).

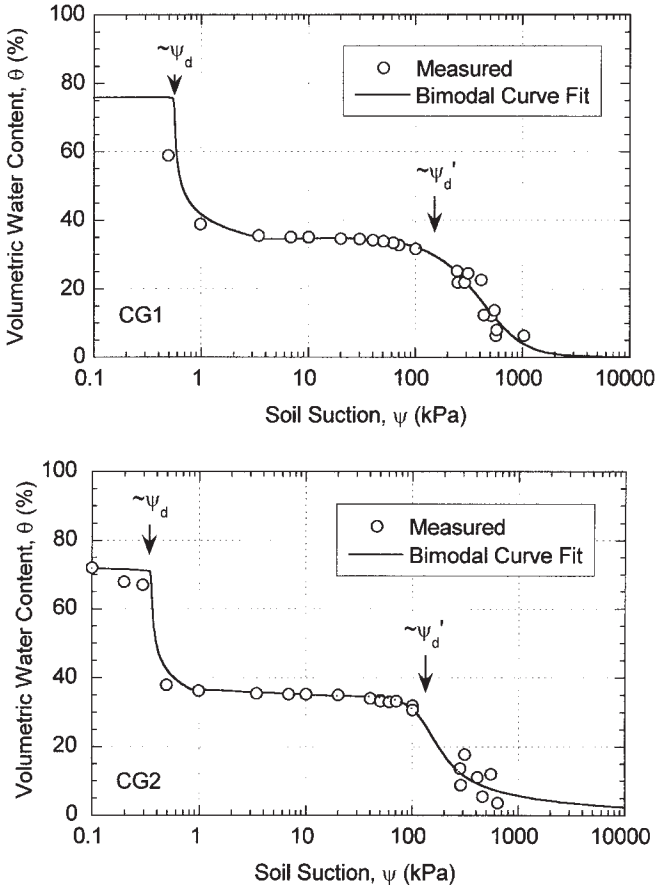

Table 3. Total, microscopic (intrapellet), and macroscopic (interpellet) porosity values from bimodal curve fits for pelletized diatomaceous earth materials CG1 and CG2.

Soil-water characteristic curve function	Total porosity, n_T	Microscopic portion		Macroscopic portion	
		Microporosity, n_m	Percent of total porosity	Macroporosity, n_M	Percent of total porosity
Material CG1					
Brooks–Corey	0.764	0.337	44.1	0.427	55.9
van Genuchten	0.764	0.344	45.0	0.420	55.0
Fredlund–Xing	0.764	0.350	45.8	0.414	54.2
Average	—	0.344	45.0	0.420	55.0
Material CG2					
Brooks–Corey	0.725	0.344	47.4	0.381	52.6
van Genuchten	0.725	0.349	48.1	0.376	51.9
Fredlund–Xing	0.725	0.350	48.3	0.375	51.7
Average	—	0.348	47.9	0.377	52.1

content, θ_j, regressed from the bimodal moisture characteristic data when all of the microscopic porosity is saturated (i.e., $n_m = \theta_j$). Therefore, the macroscopic or interpellet porosity, n_M, is assumed to be equal to the total porosity minus the microscopic or intrapellet porosity (i.e., $n_M = n_T - n_m$).

The resulting values of total porosity n_T, microscopic porosity n_m, and macroscopic porosity n_M based on each of the three bimodal function fits are listed in Table 3 along with the average values. In addition, the corresponding percentages of total porosity attributed to the microscopic and macroscopic porosities are shown.

The differences among the microscopic and macroscopic values reported in Table 3 for each material based on the three bimodal soil-water characteristic curve functions are small. For example, the microscopic porosity for CG1 varies by less than ±0.007 (±2.0%) from the average value of 0.344

Fig. 13. Comparison of air-entry suction from bimodal Brooks–Corey curve fits versus with the values for $1/\alpha$ and $1/\alpha'$ from the bimodal van Genuchten function fits and the values a and a' from the bimodal Fredlund–Xing function fits.

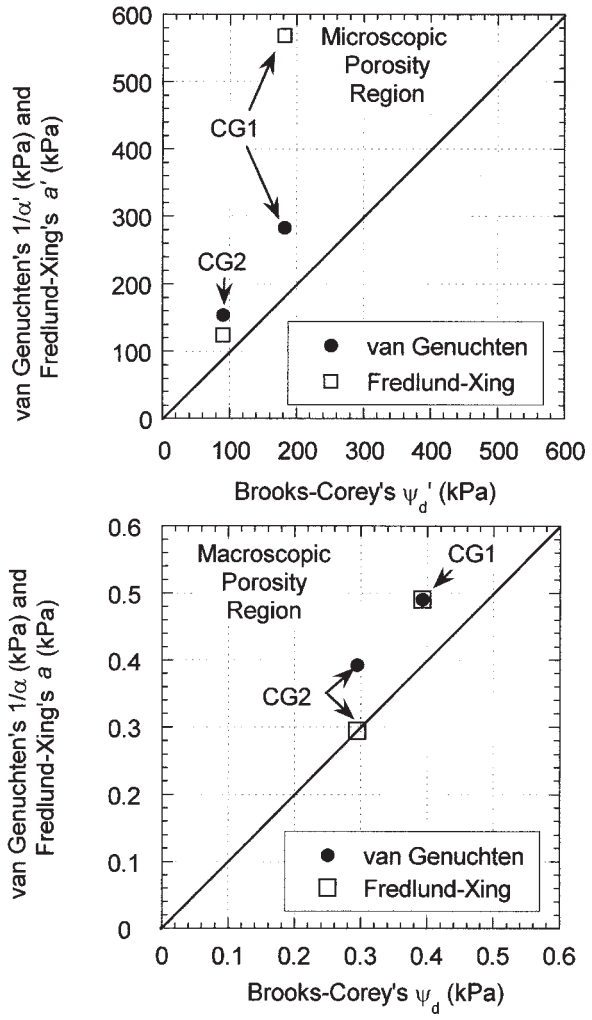

based on all three functions, whereas the microscopic porosity for CG2 varies by less than ±0.004 (±1.1%) from the average value of 0.348. Thus, the overall evaluation of the microscopic versus macroscopic portions of the diatomaceous earth specimens is essentially independent of the bimodal soil-water characteristic curve function used in the analysis.

Overall, the microscopic porosity accounts for 45.0% of the total porosity of 0.764 for the CG1 material and for 47.9% of the total porosity of 0.725 for the CG2 material based on the average value from the three functions. The microscopic porosity values are approximately equal for the CG1 and CG2 materials, as expected assuming a similar structure for the microscopic portion for the two materials. The macroscopic porosity of the CG2 material is less than that of the CG1 material, as expected on the basis of the larger pellet size for CG2. These results compare favorably with those reported by Sundine Enterprises, Inc. (1996), where approximately 50% of the total porosity is attributed to microscopic porosity based on mercury-intrusion porosimetry.

Summary and conclusions

In this study, the soil-water characteristic curves of two sizes of processed diatomaceous earth pellets were measured using a combination of methods to cover a wide range of suctions (0.1–980 kPa) and to minimize the time required for measurement of the data. The measured soil-water characteristic curves for the pelletized diatomaceous earth reflect two distinct pore-size distributions associated with the microscopic and macroscopic portions of the total porosity of the specimens. The measured soil-water characteristic curve data were fitted with the Brooks–Corey, van Genuchten, and Fredlund–Xing unimodal soil-water characteristic curve functions, which were modified to account for the observed bimodal soil-water characteristic curve data.

The soil-water characteristic curves of the two different sizes (i.e., ~1 mm and ~2 mm diameter) of diatomaceous earth pellets were similar in terms of both the microscopic and the macroscopic portions. The soil-water characteristic curve data for both pellet sizes indicate a broad range of pores sizes associated with the microscopic porosity. However, the air-entry suction based on the macroscopic portion of the specimens containing the ~2 mm diameter pellets (i.e., CG2 material) is approximately 0.1 kPa lower than that based on the macroscopic portion of the specimens containing the ~1 mm diameter pellets (i.e., CG1 material), as expected on the basis of the larger particle sizes of the CG2 material.

The method used in this study to fit bimodal soil-water characteristic curve data using existing unimodal soil-water characteristic curve functions modified to account for the bimodal nature of the soil-water characteristic curve data resulted in good fits of the measured data for all three functions. For example, the microscopic porosity for the CG1 material varied by less than ±0.007 (±2.0%) from the average value of 0.344 based on all three functions, whereas the microscopic porosity for the CG2 material varied by less than ±0.004 (±1.1%) from the average value of 0.348. Thus, the overall evaluation of the microscopic versus macroscopic portions of the total porosity of the specimens containing the diatomaceous earth pellets was essentially independent of the bimodal soil-water characteristic curve function used in the analysis.

Based on the curve fits performed in this study, the microscopic porosity accounts for an average of 45.0% of the total porosity of 0.764 for the CG1 material and 47.9% of the total porosity of 0.725 for the CG2 material. These percentages are consistent with the value of 50% reported in the product information for the same materials on the basis of mercury-intrusion porosimetry. Thus, all three modified soil-water characteristic curve functions apparently were successful at determining the microscopic and macroscopic portions of the total porosity of the two dual-porosity media used in this study.

Acknowledgments

The assistance of Robert Gilkeson and Los Alamos National Laboratory for the use of the CMP is appreciated. Also, the constructive comments from the three anonymous

reviewers and Associate Editor greatly improved the overall quality of the paper and are sincerely appreciated.

References

Breese, R.O.Y. 1994. Diatomite. *In* Industrial minerals and rocks. 6th ed. Vol. 1. Society for Mining, Metallurgy, and Exploration, Inc., Littleton, Colo., pp. 397–412.

Brooks, R.H., and Corey, A.T. 1964. Hydraulic properties of porous media. Colorado State University (Fort Collins), Hydrology Paper 3.

Chao, K.C. 1995. Hydraulic properties and heave prediction for expansive soils. MS report, Colorado State University, Fort Collins, Colo.

Chiu, T.F., and Shackelford, C.D. 1998. Unsaturated hydraulic conductivity of compacted sand–kaolin mixtures. Journal of Geotechnical and Geoenvironmental Engineering, ASCE, **124**(2): 160–170.

Day, R.W. 1995. Engineering properties of diatomaceous fill. Journal of Geotechnical Engineering, ASCE, **121**(12): 908–910.

Durner, W. 1992. Predicting the unsaturated hydraulic conductivity using multi-porosity water retention curves. *In* Proceedings of the International Workshop on Indirect Methods for Estimating the Hydraulic Properties of Unsaturated Soils. 11–13 Oct., 1989. *Edited by* M.T. van Genuchten, F.J. Leij, and L.J. Lund. University of California, Riverside, pp. 185–202.

Durner, W. 1994. Hydraulic conductivity estimation for soils with heterogeneous pore structure. Water Resources Research, **30**(2): 211–223.

Fredlund, D.G., and Rahardjo, H. 1993. Soil mechanics for unsaturated soils. John Wiley and Sons, Inc., New York.

Fredlund, D.G., and Xing, A. 1994. Equations for the soil-water characteristic curve. Canadian Geotechnical Journal, **31**: 521–532.

Gee, G.W., Campbell, M.D., Campbell, G.S., and Campbell, J.H. 1992. Rapid measurement of low soil water potentials using a water activity meter. Soil Science Society of America Journal, **56**(4): 1068–1070.

Gerke, H.H., and van Genuchten, M.T. 1993. A dual-porosity model for simulating the preferential movement of water and solutes in structured porous media. Water Resources Research, **29**(2): 305–319.

Griffioen, J.W., Barry, D.A., and Parlange, J.-Y. 1998. Interpretation of two-region model parameters. Water Resources Research, **34**(3): 373–384.

Khilnani, K., and Capik, M.L. 1989. Diatomaceous soils: a new approach. Civil Engineering, **59**(2): 68–70.

Klute, A. 1986. Water retention: laboratory methods. *In* Methods of soil analysis. Part 1: physical and mineralogical methods. 2nd ed. Agronomy Monograph 9, American Society of Agronomy, Soil Science Society of America, Madison, Wis., Chapt. 26.

Lange, K.P. 1983. Removal of giardia lamblia cysts and other substances by diatomaceous earth filtration. M.S. thesis, Colorado State University, Fort Collins, Colo.

Leong, E.C., and Rahardjo, H. 1997. Review of soil-water characteristic curve equations. Journal of Geotechnical and Geoenvironmental Engineering, ASCE, **123**(12): 1106–1117.

Lukasik, J., Farrah, S.R., Truesdail, S., and Shah, D.O. 1996. Adsorption of microorganisms to sand and diatomaceous earth particles coated with metallic hydroxides. Kona, **14**: 87–91.

Mallants, D., Tseng, P.H., Toride, N., Timmerman, A., and Feyen, J. 1997. Evaluation of multimodal hydraulic functions in characterizing a heterogeneous field soil. Journal of Hydrology, **195**(1–4): 172–199.

Maraqa, M.A., Wallace, R.B., and Voice, T.C. 1997. Effects of degree of water saturation on dispersivity and immobile water in sandy soil columns. Journal of Contaminant Hydrology, **25**: 199–218.

Meisinger, A.C. 1985. Diatomite. U.S. Bureau of Mines, Reprint from Bulletin 675.

Miller, D.J. 1996. Osmotic suction as a valid stress state variable in unsaturated soils. Ph.D. dissertation, Colorado State University, Fort Collins, Colo.

Othmer, H., Diekkruger, B., and Kutilek, M. 1991. Bimodal porosity and unsaturated hydraulic conductivity. Soil Science, **152**(3): 139–149.

Peters, R.R., and Klavetter, E.A. 1988. A continuum model for water movement in an unsaturated fractured rock mass. Water Resources Research, **24**(3): 416–430.

Pruess, K., Wang, J.S.Y., and Tsang, Y.W. 1990. On thermohydrologic conditions near high-level nuclear wastes emplaced in partially saturated fractured tuff. 2. Effective continuum approach. Water Resources Research, **26**(6): 1249–1261.

Ray, C., Ellsworth, T.R., Valocchi, A.J., and Boast, C.W. 1997. An improved dual porosity model for chemical transport in macroporous soils. Journal of Hydrology, **193**: 270–292.

Rogers, D.B., and Gallaher, B.M. 1995. The unsaturated hydraulic characteristics of the Bandelier Tuff. Los Alamos National Laboratory Report LA-12968-MS.

Ross, P.J., and Smettem, K.R.J. 1993. Describing soil hydraulic properties with the sum of simple functions. Soil Science Society of America Journal, **57**(1): 26–29.

Smettem, K.R.J., and Kirby, C. 1990. Measuring the hydraulic properties of a stable aggregated soil. Journal of Hydrology, **117**(1–4): 1–13.

Smettem, K.R.J., Chittleborough, D.J., Richards, B.G., and Leaney, F.W. 1991. The influence of macropores on runoff generation from a hillslope soil with a contrasting textural class. Journal of Hydrology, **122**(1–4): 235–252.

Stavnes, S., Yorke, C.A., and Thompson. L. 1996. In situ bioremediation of petroleum in tight soils using hydraulic fracturing. *In* Proceedings of the HazWaste World/Superfund 17th Conference, Washington, D.C.

Sundine Enterprises, Inc. 1996. Isolite product literature. Sundine Enterprises, Inc., Arvada, Colo.

van Genuchten, M.T. 1980. A closed-form equation for predicting the hydraulic conductivity of unsaturated soils. Soil Science Society of America Journal, **44**(5): 892–898.

van Genuchten, M.T., Leij, F.J., and Yates, S.R. 1991. The RETC code for quantifying the hydraulic functions of soils. EPA Report 600/2-91/065, U.S. Salinity Laboratory, U.S. Department of Agriculture, Agricultural Research Service, Riverside, Calif.

Wang, J.S.Y., and Narasimhan, T.N. 1985. Hydrologic mechanisms governing fluid flow in a partially saturated, fractured, porous medium. Water Resources Research, **21**(12): 1861–1874.

Wang, J.S.Y., and Narasimhan, T.N. 1990. Fluid flow in partially saturated, welded–nonwelded tuff units. Geoderma, **46**(1–3): 155–168.

Wilson, G.V., Jardine, P.M., and Gwo, J.P. 1992. Modeling the hydraulic properties of a multiregion soil. Soil Science Society of America Journal, **56**(6): 1731–1737.